Journal Name

ARTICLE

High Performance Non-Doped Green Organic Light Emitting Diode via Delayed Fluorescence

Received 00th January 20xx,
Accepted 00th January 20xx

DOI: 10.1039/x0xx00000x

www.rsc.org/

Bahadur Sk,[a] Vasudevan Thangaraji,[b] Nisha Yadav,[a] Gyana Prakash Nanda,[a] Sannibha Das,[a] Parthasarathy Gandeepan,*[c] Eli Zysman-Colman,*[d] and Pachaiyappan Rajamalli*[a]

Non-doped, delayed fluorescence organic light-emitting diodes (OLEDs) provide a route to high performance devices and simplified device fabrication. Here, two ambipolar anthracene derivatives containing a hole-transporting di-*p*-tolylamine and a carbazole and an electron-transporting phosphine oxide moiety were rationally designed and synthesized. The thermal and optoelectronic properties were investigated and the neat films of these compounds show high photoluminescence quantum yields of 84-87%. Non-doped OLEDs with these luminogens exhibit green emission at ~545 nm and EQE_{max} over 7.2% due to the delayed fluorescence resulting from triplet-triplet annihilation (TTA). The devices show high luminance over 104,400 cd m^{-2}. Power efficiency and current efficiency maxima are up to 23.0 lm W^{-1} and 28.3 cd A^{-1}, respectively. Moreover, the devices show very low efficiency roll-off and retain 90% of the maximum efficiency even at 20,000 cd m^{-2}. When combined with a thermally activated delayed fluorescent (TADF) assistant dopant, the green-emitting OLEDs show a high EQE_{max} of 17.8%.

1. Introduction

Organic light-emitting diode (OLED) displays have many distinct performance advantages over liquid crystal displays (LCDs) that include: fast refresh rate, wider viewing angles, facile colour tuning, a higher contrast ratio, easy access to flexible panels, and are lightweight.[1-4] It is therefore not surprising that OLEDs are the ascendant technology for displays and have now been commercialized. In the past few decades, the intensive research focuses on OLEDs and the materials that underpin them has led to significantly improved performance of the devices.[5,6] In the OLEDs using only traditional fluorescent emitters (1st generation), the radiative decay of triplet excitons (75%) is spin-forbidden and only singlet excitons (25%) can be recruited to produce light thus providing an upper-bound limit to the efficiency of the device.[7-10] Conversely, noble metal-based phosphorescent complexes (2nd generation) exhibit emissive triplet states due to singlet-triplet state mixing via efficient spin-orbit coupling mediated by the heavy metal and thus they can harvest both singlet and triplet excitons (100%) for light emission.[11-16] Although the 2nd generation phosphorescent emitters containing metals such as iridium or platinum produce devices that show very high efficiencies, these metals are scarce, and blue phosphorescent devices do not yet show either the efficiencies or the stabilities required for commercial use.

Presently, fluorescent OLEDs with materials capable of up-converting triplet excitons to singlet excitons have been investigated to overcome the internal quantum efficiency limitations of conventional fluorescence OLEDs.[17-22] Two possible up-conversion mechanisms have been reported: thermally activated delayed fluorescence (TADF)[23-31] and triplet-triplet annihilation (TTA).[32-34] TADF materials have a small singlet-triplet energy gap, ΔE_{ST}, that enables triplet excitons to undergo reverse intersystem crossing (RISC) to form singlet excitons. However, a present drawback of TADF-based OLEDs is that they frequently show significant efficiency roll-off, low device luminescence and stability.[35-37] Therefore, TTA materials with high electroluminescence (EL) efficiencies and stabilities are attractive to satisfy industrial specifications. OLED devices typically rely on emitters that are doped into hosts. The choice of a suitable host and its impact on device performance complicates the design. In this context, non-doped devices are much attractive because of their simpler device architecture and high reproducibility. Thus, the development of high performance non-doped TTA-based devices would be highly desired.

In this study we have rationally designed two ambipolar anthracene-based TTA emitters, (4-(10-(di-*p*-tolylamino)anthracen-9-yl)phenyl)diphenylphosphine oxide

[a] *Materials Research Centre, Indian Institute of Science, Bangalore-560012, Karnataka, India. E-mail: rajamalli@iisc.ac.in*
[b] *Department of Chemistry, National Tsing Hua University, Hsinchu 30013, Taiwan.*
[c] *Department of Chemistry, Indian Institute of Technology Tirupati, Tirupati, Andhra Pradesh 517506, India. E-mail: pgandeepan@iittp.ac.in*
[d] *Organic Semiconductor Centre, EaStCHEM School of Chemistry, University of St Andrews, St Andrews, United Kingdom. E-mail: eli.zysman-colman@st-andrews.ac.uk*

† Footnotes relating to the title and/or authors should appear here.
Electronic Supplementary Information (ESI) available: [General information, synthesis procedure, single crystal data, TGA, DFT Calculations, Lippert-Mataga plots, Transient decay, power efficiency vs luminance, summary of device performance at various brightness. See DOI: 10.1039/x0xx00000x

(TAA-PPO) and (4-(9*H*-carbazol-9-yl)phenyl)(4-(10-(di-*p*-tolylamino)anthracen-9-yl)phenyl)(phenyl)phosphine oxide (CzA-PPO), for use in efficient, non-doped OLEDs (Scheme 1). Here, the anthracene chromophore is selected because anthracene crystals have been reported to exhibit delayed fluorescence (DF).[38,39] Therefore, strong DF was expected to be observed when using TAA-PPO and CzA-PPO as the emitters in the OLEDs. In most of the reported TTA emitters, anthracene or pyrene moieties are decorated with either a hole transporting unit such as carbazole or an electron transporting unit such as imidazole.[32,40,41,42a] These emitters have been usually employed in doped OLEDs for smooth injection of electrons or holes into the emitting layer (EML). In these doped devices, it is important to control the dopant concentration in the EML during the device fabrication process to obtain reproducible device performance. Otherwise, it leads to a change in the emission colour or concentration quenching. Therefore, to simplify the device fabrication process and to improve the charge balance in the device, we have designed ambipolar anthracene-based emitters with hole-transporting carbazole and tolylamine units and electron-transporting phosphine oxide units. With this design, non-doped OLEDs achieved high luminance over 104,400 cd m^{-2}, which is comparable with green phosphorescent OLEDs.[42b,c] Moreover, green OLEDs based on TAA-PPO and using a TADF-based assistant dopant show record-high EQE_{max} of 17.8%.

2. Result and discussion

2.1. Synthesis and DFT calculations

The compounds TAA-PPO and CzA-PPO, shown in Scheme 1, were conveniently prepared in high yields via a palladium-catalyzed phosphination. The synthesized emitters were purified by temperature gradient vacuum sublimation. The identity and purity of the compounds were determined by a combination of ^{1}H and ^{13}C NMR spectra and high-resolution mass spectrometry (HRMS). The chemical structure of TAA-PPO was confirmed by single-crystal X-ray diffraction analysis (Fig. 1). According to the crystal structure (Table S1), the tolylamine group is twisted with respect to the anthracene core by ~70.8°. There is therefore no close-contact between adjacent anthracenes in the crystal, which suggests that there should be no excimer formation in the neat film. Moreover, the twisted conformation of the tolylamine donor to the anthracene bridge in TAA-PPO impedes intermolecular interactions that would cause self-quenching, which should therefore lead to a conservation of the high photoluminescence quantum yield in the neat film.

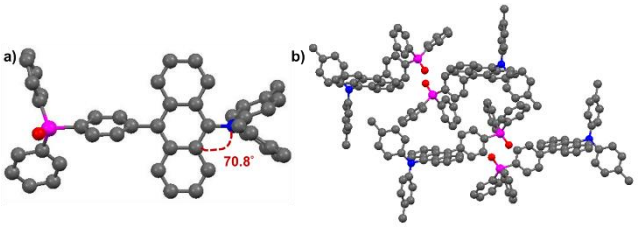

Fig. 1 The single crystal structure of TAA-PPO (a) and crystal packing (b) (hydrogen atoms have been removed for clarity).

To gain insight into the electronic structure of TAA-PPO and CzA-PPO, Density Functional Theory (DFT) calculations were performed at the B3LYP/6-31G(d,p) level of theory in vacuum. Fig. 2 shows the HOMO and the LUMO distribution of both emitters. The results reveal that the HOMO of both TAA-PPO and CzA-PPO is mainly distributed on the tolylamine unit and slightly extended on the anthracene group. The LUMO is mostly localized on the anthracene group, while the phosphine oxide essentially does not contribute to this molecular orbital. These results show that both emitters act as donor-acceptor (D–A) dipole molecules, possessing an intramolecular charge transfer character in the S_1 state resulting from a HOMO to LUMO transition. Further, hole and particles distributions were analysed to assess the nature of the excited singlet and triplet states. The holes for the S_1 states are located on the donor diphenylamine and slightly extended to anthracene while the particles are distributed only on the anthracene moiety (Fig. 3, Fig S1). This illustrates the CT character of S_1 excited state for both compounds.

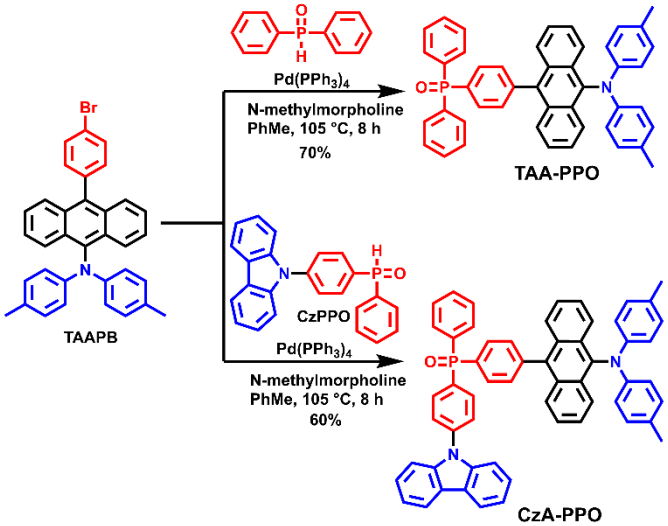

Scheme 1 Synthetic schemes of TAA-PPO and CzA-PPO.

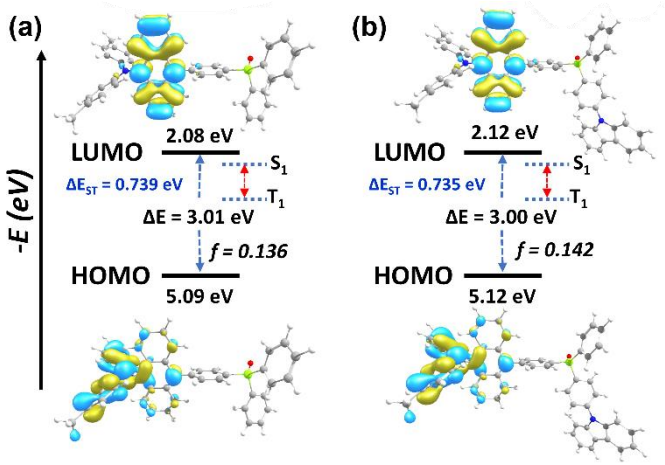

Fig. 2 Calculated electron density distribution of the HOMO and LUMO of (a) TAA-PPO and (b) CzA-PPO.

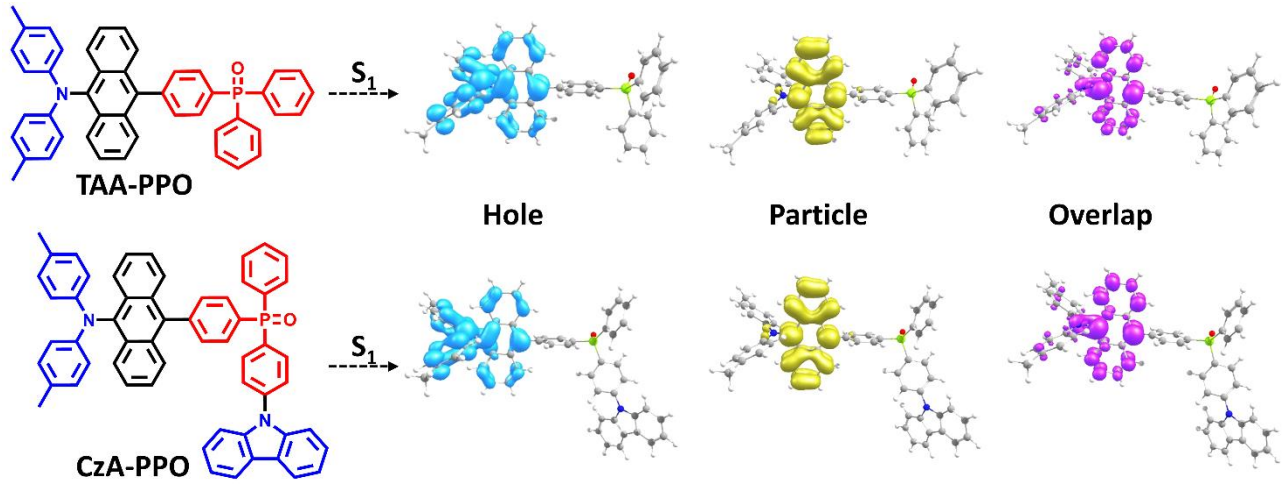

Fig. 3 The TDDFT calculated the hole–particle distributions describing the excitation characters of the S_1 of TAA-PPO and CzA-PPO are shown. The weights of the hole–particle overlap to the excitations are included. (Isovalue = 0.001)

2.2. Optoelectronic properties

As depicted in Fig. 4a, the absorption spectra of TAA-PPO in different solvents were nearly superimposable, indicating that in the ground state, there is only a small transition dipole moment. The absorption bands at 366 nm are assigned to π-π^* transitions localized on the anthracene while the broad and unstructured band at 450 nm is assigned to an intramolecular charge transfer (ICT) band.[43] This behaviour is mirrored for CzA-PPO (Fig. 4c).

The emission spectrum of TAA-PPO shifted from 490 nm in n-hexane to 551 nm in dichloromethane (DCM), with a concomitant reduction in emission intensity, thus showing a strong positive solvatochromism that is characteristic of emission from an ICT state (Fig. 4b). Similar photophysical behaviour was observed for the CzA-PPO (Fig. 4d). The solvatochromic behaviour of both compounds were analysed using Lippert-Mataga theory (Fig. S2, Table S2-S3). The larger transition dipoles in the excited state for both the compounds coupled with the linear Lippert-Mataga plots indicate that the emissive excited state is prominently intramolecular charge transfer (ICT) in character across all solvents.

The energy gaps (Eg) determined from the intersection point of the normalized absorption and the emission spectra of TAA-PPO and CzA-PPO are 2.61 and 2.64 eV, respectively. The electrochemical properties of TAA-PPO and CzA-PPO were examined by cyclic voltammetry (CV) and the results are shown in Fig. 5. No reduction wave could be detected within the dichloromethane solvent window. The HOMO energy levels were calculated to be 5.30 and 5.27 eV from the oxidation potentials of TAA-PPO and CzA-PPO, respectively. The LUMO energy levels were determined to be 2.69 and 2.63 eV for TAA-PPO and CzA-PPO, respectively. The destabilized LUMO in CzA-PPO compared to TAA-PPO results from the presence of the electron-donating carbazole unit in the former. The photophysical properties data are summarized in Table 1.

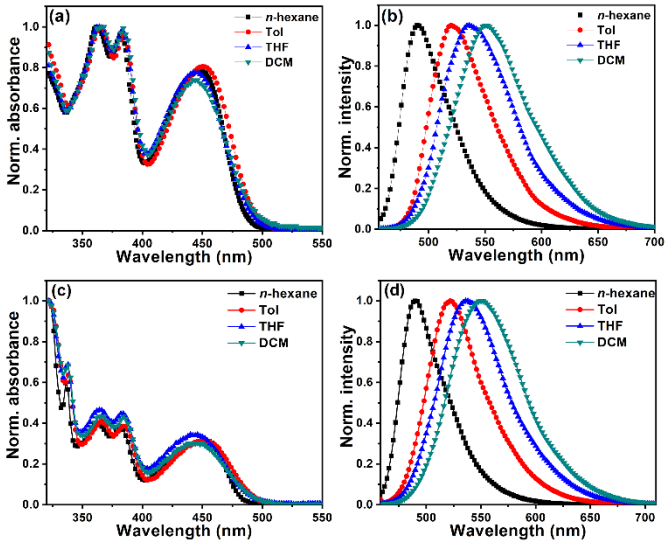

Fig. 4 Normalized absorption and emission spectra (λ_{exc} = 450 nm) of (a, b) TAA-PPO and (c, d) CzA-PPO in solvents with varying polarity at room temperature.

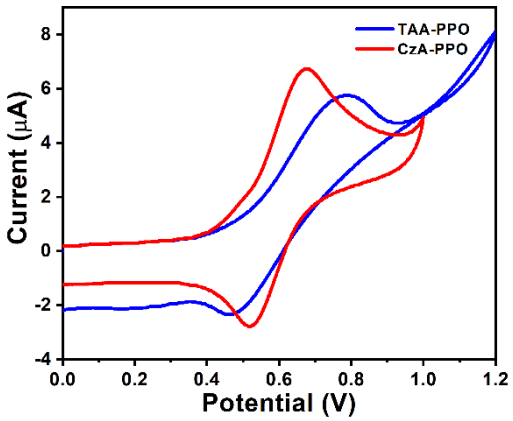

Fig. 5 Oxidation potentials of TAA-PPO and CzA-PPO in DCM reported versus Fc/Fc+.

Table 1. Optoelectronic and thermal properties of **TAA-PPO** and **CzA-PPO**.

Emitter	λ_{abs} / nm[a]	λ_{PL} / nm[a]	Φ_{PL} /% sol[b]/film[c]	T_d / °C[d]	HOMO / eV[e]	LUMO / eV[f]	E_g / eV[g]
TAA-PPO	365, 450	520	63/87	450	-5.30	-2.69	2.61
CzA-PPO	365, 452	522	68/84	417	-5.27	-2.63	2.64

[a]Absorption and photoluminescence spectra (λ_{exc} = 450 nm) measured in toluene with concentration of 10^{-5} M at 300 K. [b]Measured in toluene solution using C545T as the standard[46b]. [c]Absolute Φ_{PL} evaluated for neat film using an integrating sphere. [d]Obtained from TGA measurements. [e]Determined from the oxidation potentials in 10^{-3} M DCM solution by cyclic voltammetry (-4.8+$E_{1/2}$ (ox)-$E_{1/2}$(ox)(Fc)). [f]HOMO - E_g. [g]Obtained from intersection point of the normalized emission and absorption spectra.

Both TAA-PPO and CzA-PPO exhibit high photoluminescence quantum yields (Φ_{PL}) of 63% and 68%, respectively, in toluene. Surprisingly, the Φ_{PL} values of the non-doped films of TAA-PPO and CzA-PPO are increased to 87% and 84%, respectively, and their higher values compared to those in solution are probably due to the suppression of collisional quenching and bond rotation in the solid state.[44-46a] The emission decay of TAA-PPO in the neat thin film shows biexponential decay with τ_{PL} of 3.7 ns (36%) and 12.2 ns (64%) (Fig. S3-S4). Similarly, the emission decay of CzA-PPO exhibits biexponential decay with the lifetimes of 7.2 (41%) ns and 18.9 (59%) ns. However, no long-lived species were detected under the photoexcitation of these films. This result suggests that these emitters are conventional fluorescence emitter and is not a TADF emitter.

The thermal properties were determined by thermogravimetric analysis (TGA) to assess the thermal stabilities of the compounds (Fig. S5). Both compounds showed decomposition temperatures of over 400 °C. The high T_d values of the compounds are attractive for vacuum-sublimed devices.

2.3. Electroluminescence performance

In light of the high Φ_{PL} values in neat films, non-doped OLEDs were fabricated with the following device architecture: indium tin oxide (ITO)/ NPB (30 nm)/TCTA (20 nm)/ TAA-PPO or CzA-PPO (30 nm)/ TPBi (60 nm)/LiF (1 nm)/Al (100 nm) (Fig. 6a, 6b). Here, NPB [4,4′-*N*,*N*′-bis[*N*-(1-naphthyl)-*N*-phenylamino]biphenyl] acts as a hole injection layer while TCTA [tris[4-(9*H*-carbazol-9-yl)phenyl]amine] acts as a hole-transporting layer material. TPBi [1,3,5-tris(*N*-phenylbenzimiazole-2-yl)benzene] acts as an electron-transporting material. Devices G1 and G2 were fabricated using TAA-PPO and CzA-PPO, respectively.

The electroluminescence performances of the two non-doped OLEDs are shown in Fig. 6c and Fig. S6 and summarized in Table 2. The current (I)-voltage(V)-luminance (L) characteristics are shown in Fig. S6a and the EQE vs luminance of devices G1 and G2 are shown in Fig. 6c. Both devices showed very high luminance with values of 103,500 and 104,400 cd m^{-2} for devices G1 and G2, respectively; there was no additional light out-coupling enhancement. The EQE_{max} of devices G1 and G2 are 7.1% and 7.2%, respectively. To the best of our knowledge, there is no report of a green TTA-based non-doped

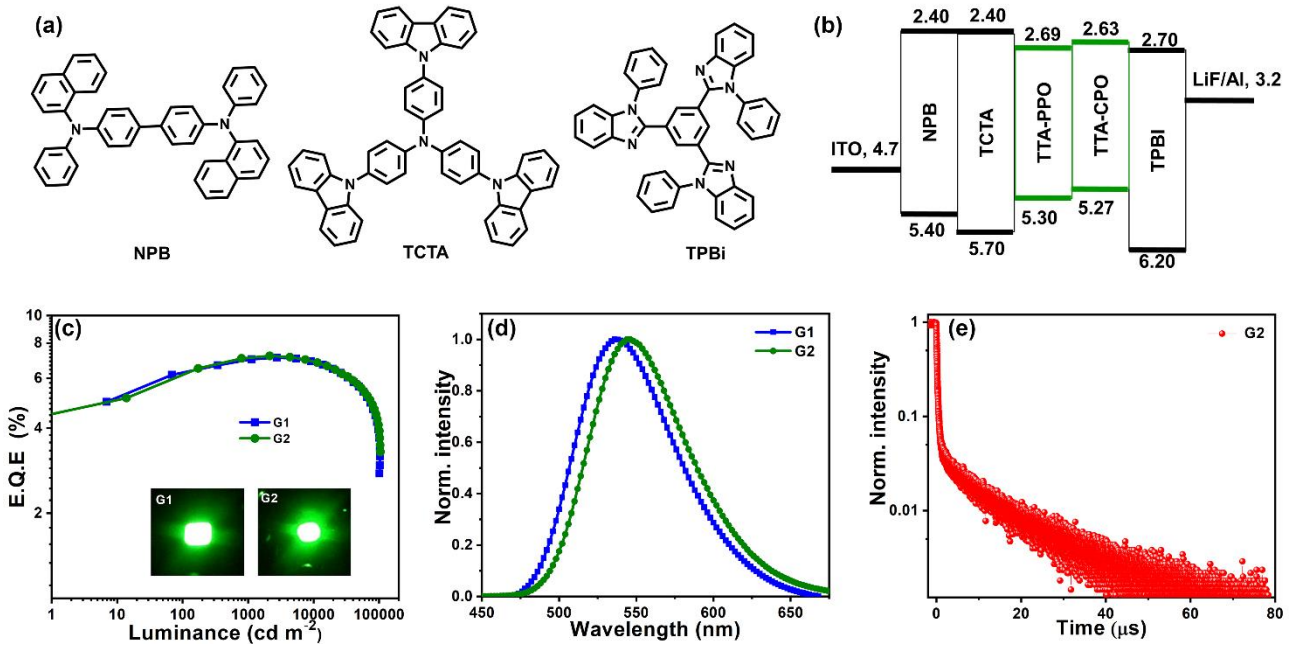

Fig. 6 Electroluminescence properties of devices G1 and G2 using TAA-PPO and CzA-PPO, respectively: (a) Chemical structures of the organic materials used in the EL devices, (b) schematic representation of device architecture, (c) external quantum efficiency vs luminance; (d) electroluminescence spectra and (e) Transient decay of the G2 device measured at 545 nm with 6 V.

Table 2. EL performances of the device G1 and G2[a].

Device[a]	Emitter	V_d /V[b]	L_{max} / cd m^{-2}, V	EQE_{max} / %, V	CE_{max} / cd A^{-1}, V	PE_{max} / lm W^{-1}	λ_{EL} / nm at 8V	CIE at 8V / (x, y)
G1	**TAA-PPO**	2.6	103500, 14.0	7.1, 5.0	27.9, 5.0	21.7, 3.5	537	0.34, 0.61
G2	**CzA-PPO**	2.5	104400, 15.5	7.2, 4.5	28.3, 4.5	23.0, 3.5	545	0.38, 0.59

[a]Device configuration: ITO/ NPB (30 nm) / TCTA (20 nm) / **TAA-PPO** or **CzA-PPO** (30 nm) / TBPi (60 nm) / LiF (1 nm) / Al (100 nm). [b]V_d, the operating voltage at a brightness of 1 cd m^{-2}. L_{max}, maximum luminance. EQE_{max}, maximum external quantum efficiency. CE_{max}, maximum current efficiency. PE_{max}, maximum power efficiency. λ_{EL}, the wavelength where the EL spectrum have the maximum intensity.

OLED with an EQE greater than 7.1%, although EQEs is 6.0% have been reported for doped devices.[40] Both devices showed low turn-on voltages of 2.6 and 2.5 V (for G1 and G2, respectively, at a luminance of 1 cd m^{-2}), this due to the ambipolar nature of the emitter. Device G2 performs slightly better across all metrics than device G1, which we ascribe to the increased hole mobility imparted by the additional carbazole unit. Fig. 6d contains the electroluminescence spectra, with maxima of 537 nm and 545 nm, respectively, for devices G1 and G2. This is comparable with the thin film PL spectra of TAA-PPO (λ_{PL} = 540 nm) and CzA-PPO (λ_{PL} = 549 nm) and no residual emission from the device. These results suggest that holes and electrons recombination take place only in the EML.

Notably, the high luminescence of these devices are comparable to state-of-the-art green PHOLEDs.[47,48] The power efficiencies of the devices are comparable with TADF-based devices at practical brightness level (1000 cd m^{-2}).[49-51] Indeed, the upper limit of the EQE of a conventional fluorescent OLED with a Φ_{PL} of 84% is calculated according to equation 1:

$$EQE_{max} = \eta_{op} \times \Phi_{PL} \times \eta_r \times \gamma \approx 0.2 \times 0.84 \times 0.25 \times 1 = 4.2\% \quad (1)$$

where η_{op} is the optical out coupling factor, Φ_{PL} is the photoluminescence quantum yield, η_r is the possibility that an exciton is formed as a singlet and γ is the charge balance factor.[52] For device G2, the calculated EQE is 4.2%; however, the

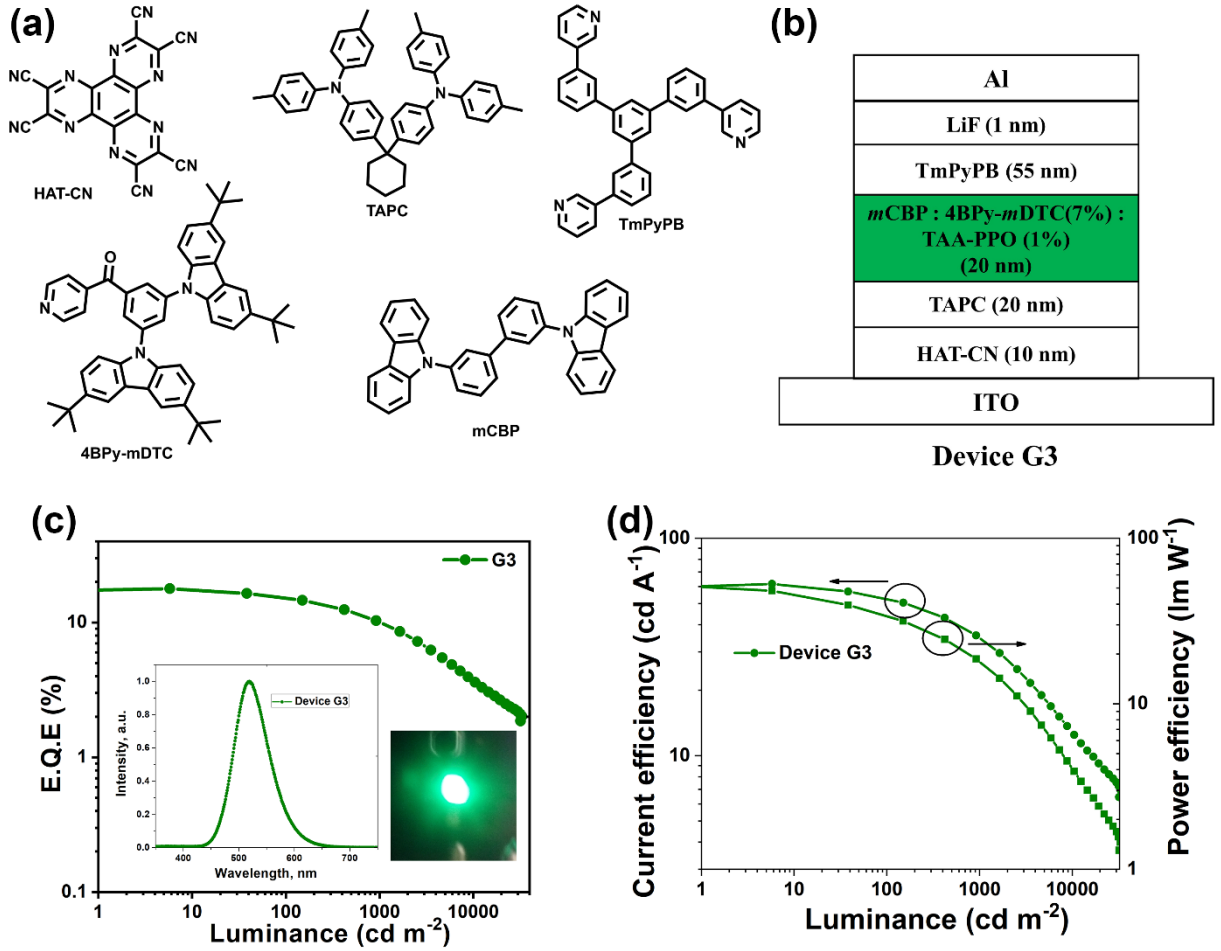

Fig. 7 (a) Chemical structures of materials used in the device G3, (b) device architecture of device G3, (c) EQE vs Luminance (insert: EL spectra), and (d) current and power efficiency vs luminance.

EQE_{max} is actually 1.7 times higher than the theoretical prediction. We ascribe the enhanced efficiency to the recruitment of triplet excitons via a TTA process, eq. 2.[32a]

$$T^1 + T^1 \rightarrow S^1 + S^0 \qquad (2)$$

The transient electroluminescence responses of device G2 is shown in Fig. 6e. A delayed electroluminescence component on the order of several tens of microseconds was observed. This clearly suggests that triplet excitons are also involved in electroluminescence.[32b] In this study, the ambipolar nature of TAA-PPO and CzA-PPO contributes to a good balance between electron and hole currents in the devices leading to efficient electron-hole recombination and exciton generation and thus high EQE. It is interesting to note that both G1 and G2 devices show increasing EQE and current efficiency as a function of increasing luminance. The results agree well with the proposed TTA phenomenon. This newly developed material design concept opens a new route for efficient non-doped TTA-based devices.

To evaluate the efficiency roll-off of these devices, the device performances were measured at a number of commercially relevant brightness levels and the data are summarized in Tables S4 and S5. Impressively, both devices G1 and G2 showed almost no roll-off from 100 to 5000 cd m^{-2} and incredibly low efficiency roll-off even at 20,000 cd m^{-2}. The EQEs at 500 and 5000 cd m^{-2} remain at 6.9 and 7.1%, respectively, for device G2; an almost similar device performance is observed for device G1. In addition, both devices retain an EQE of 6.5% at 20,000 cd m^{-2} (Table S5). The EQE of these devices is much higher than those of the reported phosphine oxide-based TADF devices (EQE ≈ 1% at 3000 cd m^{-2}) at this brightness level.[45] Although lots of TADF devices show high efficiencies (EQE_{max} over 20%), many of these OLEDs luminance never reaches 20,000 cd m^{-2}.[26, 53]

2.4. Hyperfluorescence OLED

In order to improve the EQE of the TAA-PPO OLED, a hyperfluorescence[56, 57] device architecture was employed using a TADF emitter as an assistant dopant.[45] Time-resolved spectroscopic measurements were carried out to establish the Förster resonance energy transfer (FRET) process between TADF assistant dopant and our compounds as terminal emitters. The FRET from S_1 of TADF emitter (4BPy-*m*DTC) to S_1 of TTA-PPO occurs as the absorption spectrum of TTA-PPO considerably overlaps with the emission spectrum of 4BPy-*m*DTC (Fig. 8a). Additionally, the reduction of the delayed fluorescence lifetime of 4BPy-*m*DTC in the presence of TAA-PPO indicates the prominent energy transfer from the 4BPy-*m*DTC to TAA-PPO (Fig. 8b and S7, Table S7, Scheme S1).

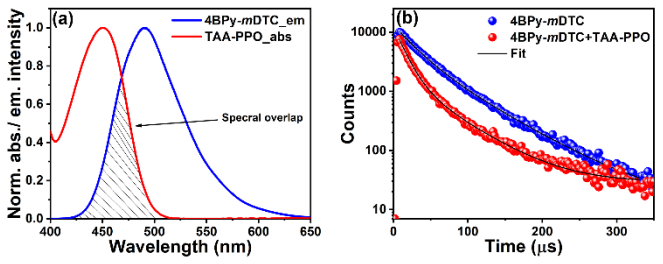

Fig. 8 (a) The spectral overlap of the emission spectrum of 4BPy-mDTC (λ_{ex} = 350 nm) and the absorption spectrum of TAA-PPO in toluene and (b) Emission decay profile of 4BPy-*m*DTC and 4BPy-*m*DTC+TAA-PPO (λ_{ex} = 350 nm, λ_{em} = 500 nm) films spin-coated using mCP host at room temperature.

Based on this, the device G3 was fabricated using the following structure: ITO/HAT-CN (10 nm)/TAPC (20 nm)/mCBP: 4BPy-*m*DTC (7 wt%):TAA-PPO (1 wt%) (20 nm)/TmPyPB (55 nm)/LiF (1 nm)/Al (100 nm). Here, 3,3-di(9*H*-carbazol-9-yl)biphenyl (*m*CBP) acts as the host material, 3,5-bis((3,6-di-*tert*-butyl-9*H*-carbazol-9-yl)phenyl)(pyridin-4-yl)methanone (4BPy-*m*DTC) serves as an assistant dopant[45] and 1,3,5-tri(*m*-pyridin-3-ylphenyl)benzene (TmPyPB) is the electron transporting material. The performance of the device G3 is summarized in Table S6, while the device architecture and compound structures are shown in Fig. 7a and 7b. Fig. 7c provides the EQE vs luminance of device G3. The device G3 shows an impressive performance with an EQE_{max} of 17.8%, demonstrating the usefulness of these compounds in this device configuration and the high efficiency of the system to harvest triplet excitons and convert these to emissive singlet excitons. In this system, electrically generated triplet excitons are created on 4BPy-*m*DTC and are up-converted to singlet excitons via RISC (Scheme S1, Fig. S7, Fig. 8). All excitons are then transferred to the singlet state of TAA-PPO via Förster resonance energy transfer and then efficiently radiatively decay from the fluorescent emitter (Scheme S1).[56] The current and power efficiencies of the device G3 are 61.6 cd A^{-1}, 48.1 lm W^{-1}, respectively. The electroluminescence spectrum demonstrates that emission occurs only from TAA-PPO, indicating that energy transfer is efficient from 4BPy-*m*DTC to TAA-PPO.

3. Experimental section

3.1. Synthesis of the target molecules

3.1.1. Synthesis of (4-(10-(di-*p*-tolylamino)anthracen-9-yl)phenyl)diphenylphosphine oxide (TAA-PPO). The diphenylphosphine oxide (DPO) (0.32 g, 1.6 mmol) 10-bromo-N,N-di-*p*-tolylanthracene-9-amine (TAAPB) (0.95 g, 1.8 mmol), N-methylmorpholine (0.27 g, 2.7 mmol), and $Pd(PPh_3)_4$ (0.369 g, 0.32 mmol) was added consecutively to 20 mL toluene under nitrogen. The reaction mixture was then heated at 105 °C for 8 h. Then the reaction mixture was cooled down to room temperature and was filtered through a short pad of Celite. The solvent was removed using rotary evaporator and the crude product was purified by silica gel column chromatography to give the desired product in 70% yield (yellow solid) and was sublimed at 320 °C (yellow crystalline solid). M.p.: 323 °C; ^{1}H NMR (400 MHz, $CDCl_3$): δ 8.19 (d, J = 8.8 Hz, 2 H), 7.81-7.91(m, 6 H), 7.52-7.62 (m, 10 H), 7.29-7.38 (m, 4 H), 6.94-7.00 (m, 8 H), 2.22 (s, 6 H)); ^{13}C NMR (100 MHz, $CDCl_3$): δ 145.4, 142.9, 142.8, 138.0, 135.6, 132.8, 132.5, 132.1, 132.2, 132.1, 132.0, 131.8, 131.6, 131.5, 131.4, 131.0, 130.3, 130.2, 129.6, 128.6, 128.5, 127.0, 126.3, 125.6, 124.6, 120.0, 20.5, 20.5; HRMS (EI^+) calcd for $C_{46}H_{36}NOP$ 649.2535, found 649.2537.

3.1.2. Synthesis of (4-(9*H*-carbazol-9-yl)phenyl)(4-(10-(di-*p*-tolylamino)anthracen-9-yl)phenyl)(phenyl) phosphine oxide (CzA-PPO). The (4-(9*H*-carbazol-9-yl)phenyl)(phenyl)phosphine oxide (CzPPO) (0.60 g, 1.6 mmol) (see supporting information for the synthesis of CzPPO), TAAPB (0.95 g, 1.8 mol), and N-methylmorpholine (0.27 g, 2.7 mmol) and $Pd(PPh_3)_4$ (0.369 g, 0.32 mmol) was added consecutively to 20 mL toluene under nitrogen. The reaction mixture was then heated at 105 ℃ for 8 h. Then the reaction mixture was cooled down to room temperature and was filtered through a short pad of Celite. The solvent was removed using rotavapor and the crude product was purified by silica gel column chromatography to give the desired product in 60% yield (red solid) and was sublimed at 340 °C (red glassy solid). M.p.: 227 °C; ^{1}H NMR (400 MHz, $CDCl_3$): δ 8.21-8.13 (m, 4 H), 8.06- 7.92 (m, 6 H), 7.81-7.79 (m, 2 H), 7.67-7.62 (m, 7 H), 7.52-7.54 (d, J = 8.4 Hz, 2 H), 7.44-7.31(m, 8 H), 7.00-6.97 (m, 8 H), 2.23 (s, 6 H); ^{13}C NMR (100 MHz, $CDCl_3$): δ 142.06, 142.03, 140.36, 133.15, 133.12, 132.84,132.72, 131.81, 131.03, 130.92, 130.83, 130.80,129.84, 129.43, 129.30, 127.27, 127.15, 126.47, 124.04, 120.91, 120.72, 109.89, 14.46. HRMS (ESI) calcd for $C_{58}H_{44}N_2OP$ $[M+H]^+$ 815.3191, found 815.3230.

4. Conclusions

In summary, two anthracene-based donor-acceptor emitters containing hole-transporting ditolylamine and electron-transporting phosphine oxide moieties were designed and synthesized. They possess excellent thermal stability with the decomposition temperature higher than 450 °C. These emitters have excited states showing intramolecular charge transfer character with high Φ_{PL} of 84-87% in neat films. The non-doped OLED devices show very low turn-on voltages 2.5 V and high luminance of 104,400 cd m^{-2} for Device G2. The EQE reached over 7.2% with current efficiencies as high as 28 cd A^{-1} and power efficiencies as high as 23 lm W^{-1}. The enhancement of the EQE beyond the theoretical limit of 5% for fluorescent OLEDs was shown to be due to the contribution from the delayed fluorescence arising from TTA. Notably, the EQE of the device retains over 6.5% at luminance of 20,000 cd m^{-2} and these results show that highly efficient fluorescent devices can be realized with a simple device structure by suitably designed TTA emitters. Furthermore, a record high device performance 17.8% of EQE_{max} has been achieved from TAA-PPO using a TADF material as an assistant dopant.

Acknowledgements

The authors are grateful to Prof. Chien-Hong Cheng, National Tsing Hua University, Taiwan, for providing facilities for OLED device fabrication and characterization. P. G. thanks the Science & Engineering Research Board (SERB), India, for the Start-up Research Grant (SRG) (Grant No: SRG/2020/000161). E.Z-C. thanks the Engineering and Physical Sciences Research Council (EPSRC) EP/P010482/1 for support. P. R. thanks the Indian Institute of Science (IISc) for generous financial support and the Science & Engineering Research Board (SERB), India, for the SERB-Power Grant (SPG) (Grant No: SPG/2020/000107). B.S. thank IISc for the C. V. Raman Fellowship under the Institute of Eminence (IoE).

Notes and references

1 Y.-F. Liu, J. Feng, Y.-G. Bi, D. Yin and H.-B. Sun, *Adv. Mater. Technol.* 2019, **4**, 1800371.
2 M. Choi, Y. J. Park, B. K. Sharma, S.-R. Bae, S. Y. Kim and J.-H. Ahn, *Sci. Adv*, 2018, **4**, 8721.
3 H. S. Nalwa, L. S. Rohwer, Handbook of Luminescence, Display Materials and Device, American Scientific Publishers, USA, 2003.
4 C. W. Tang and S. A. Van Slyke, *Appl. Phys. Lett.* 1987, **51**, 913.
5 J. H. Burroughes, D. D. C. Bradley, A. R. Broun, R. N. Marks, K. Mackay, R. H Friend, P. L. Burn and A. B. Holmes, *Nature* 1990, **347**, 539.
6 Z. Xu, B. Z. Tang, Y. Wang and D. Ma, *J. Mater. Chem. C*, 2020, **8**, 2614.
7 A. Salehi, C. Dong, D.-H. Shin, L. Zhu, C. Papa, A. Thy Bui, F. N. Castellano and F. So, *Nat. Commun.*, 2019, **10**, 2305.
8 S. H. Lin, F. I. Wu, H. Y. Tsai, P. Y. Chou, H. H. Chou, C. H. Cheng, and R. S. Liu, *J. Mater. Chem.* 2011, **21**, 8122.
9 Y. H. Chen, H. H. Chou, T. H. Su, P. Y. Chou, F. I. Wu and C. H. Cheng, *Chem. Commun.* 2011, **47**, 8865.
10 Y. Xu, X. Liang, Y. Liang, X. Guo, M. Hanif, J. Zhou, X. Zhou, C. Wang, J. Yao, R. Zhao, D. Hu, X. Qiao, D. Ma and Y. Ma, *ACS Appl. Mater. Interfaces*, 2019, **11**, 31139.
11 H. Yersin, and W. J. Finkenzeller, Highly Efficient OLEDs with Phosphorescent Materials *Wiley-VCH*, 2008.
12 K. Y. Lu, H. H. Chou, C. H. Hsieh, Y. H. O. Yang, H. R. Tsai, H. Y. Tsai, L. C. Hsu, C. Y. Chen, I. C. Chen and C. H. Cheng, *Adv. Mater.* 2011, **23**, 4933.
13 B. Minaev, G. Baryshnikov and H. Agren, *Phys. Chem. Chem. Phys*., 2014, **16**, 1719.
14 M. A. Baldo, M. E. Thompson and S. R. Forrest, *Nature*, 2000, **403**, 750.
15 T.-Y. Li, J. Wu, Z.-G. Wu, Y.-X. Zheng, J.-L. Zuo and Y. Pan, *Coord. Chem. Rev.*, 2018, **374**, 55.
16 L. Xiao, Z. Chen, B. Qu, J. Luo, S. Kong, Q. Gong and J. Kido, *Adv. Mater.* 2011, **23**, 926.
17 A. P. Monkman, *ISRN Mater. Sci.* **2013**, ID 670130.
18 X. Cui, J. Zhao, Y. Zhou, J. Ma and Y. Zhao, *J. Am. Chem. Soc.* 2014, **136**, 9256.
19 C. Ganzorig and M. Fujihira, *Appl. Phys. Lett.* 2002, **81**, 3137.
20 Y. C. Simon and C. Weder, *J. Mater. Chem.* 2012, **22**, 20817.
21 S. Sinha and A. P. Monkman, *Appl. Phys. Lett.* 2003, **82**, 4651.
22 V. Jankus, C. J. Chiang, F. Dias and A. P. Monkman, *Adv. Mater.* 2013, **25**, 1455.
23 P. Rajamalli, N. Senthilkumar, P. Y. Huang, C. C. Ren-Wu, H. W. Lin and C. H. Cheng, *J. Am. Chem. Soc.* 2017, **139**, 10948.
24 P. Rajamalli, N. Senthilkumar, P. Gandeepan, C. Z. Ren-Wu, H. W. Lin and C. H. Cheng, *J. Mater. Chem. C* 2016, **4**, 900.
25 H. Uoyama, K. Goushi, K. Shizu, H. Nomura and C. Adachi, *Nature* 2012, **492**, 234.
26 M. Y. Wong and E. Zysman-Colman, *Adv. Mater.* 2017, **29**, 1605444.
27 P. Lundberg, Y. Tsuchiya, E. M. Lindh, S. Tang, C. Adachi and L. Edman, *Nat. Commun.* 2019, **10**, 1.
28 P. Rajamalli, N. Senthilkumar, P. Gandeepan, C. C. Ren-Wu, H. W. Lin and C. H. Cheng, *ACS Appl. Mater. Interfaces* 2016, **8**, 27026.
29 B. Yurash, H. Nakanotani, Y. Olivier, D. Beljonne, C. Adachi and T. Q. Nguyen, *Adv. Mater.* 2019, **31**, 1804490.
30 S. M. Suresh, E. Duda, D. Hall, Z. Yao, S. Bagnich, A. M. Z. Slawin, H. Bassler, D. Beljonne, M. Buck, Y. Olivier, A. Köhler and E. Z. Colman. *J. Am. Chem. Soc.* 2020, **142**, 6588.
31 T.-L. Wu, M.-J. Huang, C.-C. Lin, P.-Y. Huang, T.-Y. Chou, R.-W. Chen-Cheng, H.-W. Lin, R.-S. Liu and C.-H. Cheng, *Nature Photon.*, 2018, **12**, 235.

32 a) P. Y. Chou, H. H. Chou, Y. H. Chen, T. H. Su, C. Y. Liao, H. W. Lin, W. C. Lin, H. Y. Yen, I. C. Chen and C. H. Cheng, *Chem. Commun.* 2014, **50**, 6869; b) Y.-H. Chen, C.-C. Lin, M.-J. Huang, K. Hung, Y.-C. Wu, W.-C. Lin, R.-W. Chen-Cheng, H.-W. Lin and C.-H. Cheng, *Chem. Sci.*, 2016, **7**, 4044.

33 K. Xu, J. Zhao, D. Escudero, Z. Mahmood and D. Jacquemin, *J. Phys. Chem. C*, 2015, **119**, 23801.

34 N. A. Kukhta, T. Matulaitis, D. Volyniuk, K. Ivaniuk, P. Turyk, P. Stakhira, J. V. Grazulevicius and A. P. Monkman, *J. Phys. Chem. Lett.*, 2017, **8**, 6199.

35 W. Li, Y. Pan, R. Xiao, Q. Peng, S. Zhang, D. Ma, F. Li, F. Shen, Y. Wang, B. Yang and Y. Ma, *Adv. Funct. Mater.* 2014, **24**, 1609.

36 V. Gray, D. Dzebo, A. Lundin, J. Alborzpour, M. Abrahamsson, B. Albinsson and K. M. Poulsen, *J. Mater. Chem. C*, 2015, **3**, 11111.

37 C. Murawski, K. Leo and M. C. Gather, *Adv. Mater.* 2013, **25**, 6801.

38 R. G. Kepler, J. C. Caris, P. Avakian and E. Abramson, *Phys. Rev. Lett.* 1963, **10**, 400.

39 B. Nickel, H. E. Wilhelm and A. A. Ruth, *Chem. Phys.* 1994, **188**, 267.

40 C. J. Chiang, A. Kimyonok, M. K. Etherington, G. C. Griffiths, V. Jankus, F. Turksoy and A. P. Monkman, *Adv. Funct. Mater.* 2013, **23**, 739.

41 G. Mu, S. Zhuang, W. Zhang, Y. Wang, B. Wang, L. Wang and X. Zhu, *Org. Electron.* 2015, **21**, 9.

42 a) P. Rajamalli, P. Gandeepan, M. J. Huang and C. H. Cheng, *J. Mater. Chem. C* 2015, **3**, 3329; b) K.-Y. Lu, H.-H. Chou, C.-H. Hsieh, Y.-H. O. Yang, H.-R. Tsai, H.-Y. Tsai, L.-C. Hsu, C.-Y. Chen, I-C. Chen, and C.-H. Cheng, *Adv. Mater.* 2011, **23**, 4933; c) Y.-Y. Lyu, J. Kwak, W. S. Jeon, Y. Byun, H. S. Lee, D. Kim, C. Lee, and K. Char, *Adv. Funct. Mater.* 2009, **19**, 420.

43 R. N. Jones, *Chem. Rev.*, 1947, **41**, 353.

44 S. Gan, W. Luo, B. He, L. Chen, H. Nie, R. Hu, A. Qin, Z. Zhao and B. Z. Tang, *J. Mater. Chem. C* 2016, **4**, 3705.

45 P. Rajamalli, V. Thangaraji, N. Senthilkumar, C. C. Ren-Wu, H. W. Lin and C. H. Cheng, *J. Mater. Chem. C* 2017, **5**, 2919.

46 a) P. Rajamalli, N. Senthilkumar, P. Gandeepan, P. Y. Huang, M. J. Huang, C. Z. Ren-Wu, C. Y. Yang, M. J. Chiu, L. K. Chu, H. W. Lin and C. H. Cheng, *J. Am. Chem. Soc.* 2016, **138**, 628; b) K. Okumoto, H. Kannoa, Y. Hamaa, H. Takahashi, and K. Shibata, *Appl. Phys. Lett.* 2006, **89**, 063504.

47 W. Li, Y. Pan, L. Yao, H. Liu, S. Zhang, C. Wang, F. Shen, P. Lu, B. Yang and Y. Ma, *Adv. Optical Mater*. 2014, **2**, 892.

48 C. H. Shih, P. Rajamalli, C. A. Wu, M. J. Chiu, L. K. Chu and C. H. Cheng, *J. Mater. Chem. C* 2015, **3**, 1491.

49 D. Zhang, C. Zhao, Y. Zhang, X. Song, P. Wei, M. Cai and L. Duan, *ACS Appl. Mater. Interfaces* 2017, **9**, 4769.

50 D. H. Kim, K. Inada, L. Zhao, T. Komino, N. Matsumoto, J. C. Ribierre and C. Adachi, *J. Mater. Chem. C,* 2017, **5**, 1216.

51 M. J. Sung, H. Chubachi, R. Sato, M. K. Shin, S. K. Kwon, Y. J. Pu and Y. H. Kim, *J. Mater. Chem. C* 2017, ***5***, 1090.

52 S. Nowy, B. C. Krummacher, J. Frischeisen, N. A. Reinke and W. Brütting, *J. Appl. Phys.* 2008, **104**, 123109.

53 D. R. Lee, M. Kim, S. K. Jeon, S. H. Hwang, C. W. Lee and J. Y. Lee, *Adv. Mater.* 2015, **27**, 5861.

54 T. L. Wu, M. J. Huang, C. C. Lin, P. Y. Huang, T. Y. Chou, R. W. Chen-Cheng, H. W. Lin, R. S. Liu and C. H. Cheng, *Nat. Photonics* 2018, **12**, 235.

55 M. Kim, S. K. Jeon, S. H. Hwang and J. Y. Lee, *Adv. Mater.* 2015, **27**, 2515.

56 H. Nakanotani, T. Higuchi, T. Furukawa, K. Masui, K. Morimoto, M. Numata, H. Tanaka, Y. Sagara, T. Yasuda and C. Adachi, *Nat. Commun.* 2014, **5**, 4016.

57 S. H. Han and J. Y. Lee, *J. Mater. Chem. C*, 2018, **6**, 1504.